Adsorption (2015) 21:373–381
DOI 10.1007/s10450-015-9677-5

Preparation of CuCl@AC with high CO adsorption capacity and selectivity from CO/N_2 binary mixture

Yan Huang[1] · Ying Tao[2] · Liang He[2] · Yu Duan[3] · Jing Xiao[3] · Zhong Li[1]

Received: 5 November 2014 / Revised: 7 May 2015 / Accepted: 31 May 2015 / Published online: 5 June 2015

Abstract The objective of this work is to develop CuCl@AC adsorbent with high CO capacity and selectivity from CO/N_2 binary gas mixture. A series of CuCl@AC adsorbents were prepared by a solid-state auto dispersion method, and then characterized by N_2 adsorption test, XRD and XPS. CO and N_2 adsorption isotherms on the adsorbents were measured by a volumetric method. The adsorption isotherms and selectivities of CuCl@AC adsorbents for CO/N_2 binary mixture were estimated on the basis of ideal adsorbed solution theory (IAST). Results showed that (a) CO uptakes of CuCl@AC increased with CuCl loading in the loading range of 0–1.2 g/g. The maximal CO adsorption capacity of the CuCl@AC with CuCl loading of 1.2 g/g reached 38 cc/g at the P/P_0 of 0.40, around 8 times of that over the original AC; (b) calcination time for the preparation of Cu(I)@AC had significantly impact on CO adsorption of the adsorbents due to valence change of Cu species on carbon surfaces. XPS analysis indicated that when the calcination time was optimized to be 1 h at 350 °C under argon, the prepared Cu(I)@AC had the highest percentage of Cu^+ species on its surfaces, and consequently it had the highest CO capacity among the adsorbents since adsorptive species responsible for CO adsorption is Cu^+; (c) The IAST-predicted CO/N_2 adsorption selectivities of 1.2CuCl/AC decreased with pressure. Its CO/N_2 selectivity was up to 100–450 at low pressure range of 0–10 kPa, and it remained in the range of 50–100 at higher pressure range of 20–100 kPa. The high adsorption capacity and selectivity of Cu(I)@AC adsorbents made it a promising adsorbent for CO/N_2 mixture separation.

Keywords CuCl@AC · CO adsorption · Adsorbent · Selectivity

1 Introduction

With the gradual depletion of fossil fuel and the rapid expanding energy requirements, the development of new strategies with regards to the efficient production of energy resources becomes more critical and urgent (Song 2002; Lithoxoos et al. 2010). In this scenario, CO attracted great attention due to its wide application as raw materials in chemical industry, such as Fisher–Tropsch synthesis for hydrocarbon production (Ma et al. 2010). CO can be obtained from various industrial flue gases, such as yellow phosphorus tail gas, calcium carbide furnace gas, carbon black tail gas, coke oven gas, blast furnace gas, etc. The estimated annual total CO emission from industry is over 50 Mt in China (Lu). However, in the flue gases, CO is generally presented in gas mixtures, such as CO/N_2 mixture in carbon black tail gas and blast furnace gas (García et al. 2012, Munusamy et al. 2012). Therefore, the separation and purification of CO from gas mixtures play a vital role for CO recycling and utilization.

✉ Jing Xiao
cejingxiao@scut.edu.cn

✉ Zhong Li
cezhli@scut.edu.cn

[1] School of Chemistry and Chemical Engineering, South China University of Technology, Guangzhou 510640, China

[2] Research & Development Center, China Tobacco Yunnan Industrial, Co., LTD, Kunming 650231, China

[3] Key Laboratory of Enhanced Heat Transfer and Energy Conservation of the Ministry of Education, South China University of Technology, Guangzhou 510640, China

Adsorption is considered to be one of the most promising technologies for the separation and purification of CO (Izumi et al. 2005) as it is able to selectively adsorb or accumulate CO from gas mixture over an adsorbent under ambient conditions (Rakić et al. 2005; Park et al. 2014; Xiao et al. 2013). For an effective adsorption technology, adsorbent plays the key role (Xiao et al. 2014). Till now, developed adsorbents for CO adsorption include zeolites (Wirawan and Creaser 2006; Delgado and Arean 2011), reduced metals (Iyuke et al. 2000; Miyajima et al. 2005), carbon materials (Grande et al. 2008; Lopes et al. 2009; Čičmanec et al. 2013), metal organic frameworks (Chavan et al. 2009; Leclerc et al. 2011; Chowdhury et al. 2012), soft nanoporous crystal (Sato et al. 2014), etc. Among these, carbon materials and functional carbon materials show great promises due to its rich abundance, low cost, as well as rich porosity and tunable functionalities (Xiao et al. 2008; Liu et al. 2002). Lithoxoos et al. (2010) studied CO/N_2 separation over single walled carbon nanotubes, and reported that the CO adsorption capacity of the carbon nanotube was less than 0.03 molecules/Å3, and the CO/N_2 adsorption selectivity was about 1. Grande et al. (2008) studied the separation of off-gases from steam methane reforming on activated carbon, and reported CO adsorption capacity of 0.2 mmol/g at 0.2 bar and 0.7 mmol/g at 1 bar, and CO/N_2 adsorption selectivity of 2.3 at 303 K. Lopes et al. (2009) studied CO/N_2 separation on activated carbon and zeolite. It was reported that CO adsorption capacity and CO/N_2 adsorption selectivity of activated carbon were 0.4 mmol/g and 1.3 at 1 bar, respectively, and those of zeolite were 0.8 mmol/g and 2.7 at 1 bar. Sethia et al. (2010) studied equilibrium and dynamic adsorption of CO and N_2 on ZSM-5 with different SiO_2/Al_2O_3 ratio, and reported that CO/N_2 adsorption selectivity decreased with SiO_2 ratio in ZSM-5 and were in the range of 1–2. In order to improve CO adsorption of an adsorbent, Al-Khatib et al. (2002) used an aqueous solution of $SnCl_2H_2O$ to impregnate activated carbon, and reported that the impregnated activated carbon showed a very good adsorption ability of CO gas compared to the unimpregnated sample, and the adsorptive species responsible for CO gas adsorption was confirmed to be SnO_2 instead of SnO due to the former's comparative thermodynamic stability. Czakkel et al. (2009) used aqueous solutions of Cu^{2+} and Sn^{2+} salts to impregnate activated carbon, and reported that activated carbon impregnated with Sn^{2+} salt had higher CO capacity than that impregnated with Cu^{2+} salt.

π-Complexation adsorbent (Cheng and Yang 1995; Cho et al. 2005) is a type of highly selective adsorbents to separate л electron-containing adsorbate from mixtures, such as olefin/paraffin separation and purification (Takahashi et al. 2002) and organosulfur removal from fuels (Yang et al. 2003, 2008), etc. π-complexation bonds are generally stronger than van der Waals and electrostatic interactions, and thus give rise to higher selectivities (Yang et al. 2003). To enhance the separation efficiency of CO from CO/N_2 mixture, carbon adsorbent can be impregnated with transition metal ions, such as Cu(I), which is able to form π-complexation with CO. To the best of our knowledge, the study of Cu(I)-functionalized carbon adsorbent for CO/N_2 separation was rarely reported in the literature.

Herein, a series of adsorbents Cu(I)@AC were prepared using a solid-state auto dispersion method, and then characterized by N_2 adsorption test, X-ray powder diffraction (XRD) and X-ray photoelectron spectroscopy (XPS). CO and N_2 adsorption isotherms on the adsorbents were measured by a volumetric method. The adsorption selectivities of the prepared adsorbents for CO/N_2 were estimated on the basis of ideal adsorbed solution theory (IAST). Effects of Cu(I) loading and calcination time on the textural properties and surface chemistry as well as CO adsorption of prepared Cu(I)@AC adsorbent were discussed and further reported here.

2 Experimental

2.1 Preparation of CuCl@AC adsorbents

Activated carbon (AC) was provided by XF NANO, INC, which was washed with excess amount of distilled water before use. CuCl@AC adsorbents were prepared by the solid-state auto dispersion method (Xie 1997). CuCl powder (97 %, Tianjing Damao chemical reagent Co., Ltd) was mixed with AC at a given ratio, hexane (97 %, Guangdong Guanghua Sci-Tech Co., Ltd) was added into the above solution and stirred for 10 min. The slurry was filtered, and vacuum dried at 323 K for 12 h. The sample was calcined at 623 K for 0.5–4 h under argon. After that, the sample was sealed for use.

2.2 Characterization of the adsorbents

2.2.1 N_2 adsorption test

Nitrogen adsorption isotherms were measured at 77 K on the Micromeritics ASAP 2020 equipped with commercial software of calculation and analysis. The samples were outgassed at 423 K for 8 h before measurement. The pore textural properties such as specific Langmuir and BET surface area, and pore volume were obtained by analyzing the N_2 adsorption/desorption isotherms. The pressure ranges used for the BET surface area calculations were $0.06 < P/P_0 < 0.2$.

2.2.2 X-ray diffraction (XRD)

XRD measurements were performed on a Bruker D8 Advance X-ray diffractometer with Cu Kα1 radiation ($\lambda = 1.54056$).

2.2.3 X-ray photoelectron spectroscopy (XPS)

XPS characterization was carried out on an Axis Ultra DLD spectrometer with Al Kα radiation with energy of 1486.6 eV.

2.3 Measurement of CO adsorption isotherms

CO adsorption experiments were measured on the Micromeritics ASAP 2020 at varying pressure up to 800 torr and 298 K with a standard static volumetric technique. About 80 mg of sample was degassed at 423 K in vacuum for 8 h before each run. This degas process was chosen based on the previous study (Chowdhury et al. 2009) and had proved to be efficient. The purity of CO used was 99.99 %.

3 Results and discussion

3.1 Textural parameters of adsorbents CuCl@AC

Table 1 lists the textural parameters of adsorbents CuCl@AC with various CuCl loading. The data indicated that BET surface area of these adsorbents CuCl@AC decreased with the CuCl loadings, suggesting that CuCl had been loaded into the pores of AC predominantly. For example, when CuCl loading was up to 1.6 g/g, the BET surface area of the adsorbents decreased to 198.7 from 1400.7 m^2/g, and total pore volume decreased to 0.10 from 0.66 cm^3/g. The higher the CuCl loading, the more surface area and pore volume were occupied by CuCl, which may eventually result in the pore blockage of AC.

3.2 Effect of CuCl loading on CO and N_2 adsorption

Figure 1 presents the isotherms of CO over CuCl@AC adsorbents at 298 K. Compared to the original AC, CuCl@AC adsorbents showed significantly enhanced CO adsorption capacities, implying the loading of CuCl onto AC surfaces is an effective method to enhance CO adsorption. It was also noted that the equilibrium amounts adsorbed of CO on the original AC increased almost linearly with P/P_0, suggesting a relatively weak CO adsorption affinity to AC surface. Different from original AC, CO isotherms of CuCl@AC exhibited I-type of isotherms. CO adsorption capacity increased exponentially with P/P_0 at low P/P_0 range, which was the evidence of CO strong adsorption on the surfaces of CuCl@AC. The enhanced CO adsorption capacity can be ascribed to the formation of strong adsorption sites due to the loading of Cu(I) onto AC surfaces, which adsorbed CO strongly via π-complexation (Xiao et al. 2010).

It was observed from Fig. 1a that CO equilibrium uptakes of CuCl@AC increased with CuCl loading in the loading range of 0–1.2 g/g. At the CuCl loading of 1.2 g/g, the CO adsorption capacity reached the maximal values. After that, a further increase in CuCl loading resulted in a decrease in CO adsorption capacity of CuCl@AC with CuCl loading of 1.6 g/g, as shown in Fig. 1a. This phenomenon can be attributed to the following reasons. On one hand, with increasing CuCl loading, the surface active sites of CuCl@AC adsorbents for CO adsorption increased, which would improve CO capacity of the adsorbents, and on the other hand, it led to a decrease in the surface area of the adsorbents as indicated in Table 1, which would reduce CO capacity of the adsorbents. As a result, there was an optimum CuCl loading. The optimum CuCl loading was 1.2 g/g in this work. To sum up, both BET surface area and CuCl loading of CuCl@AC adsorbents contributed to the CO adsorption capacity. To get further well-understanding of CuCl loading influence on CO adsorption of CuCl@AC, the CO isotherms based on per unit mass of adsorbent in Fig. 1a were converted into the CO isotherms based on per unit surface area, as shown in Fig. 1b. It can be seen from Fig. 1b that the equilibrium uptakes of CO per surface area of CuCl@AC adsorbents were in proportion to their loadings of CuCl. The higher CuCl loadings can improve the equilibrium uptakes of CO per surface area in the loading range of 0–1.6.

Table 1 Textural properties of CuCl@AC adsorbents with different CuCl loadings

CuCl loading (g/g)	BET surface area (m^2/g)	Total pore volume (Cm^3/g)
0	1400.7	0.66
0.1	1294.0	0.63
0.4	914.1	0.45
0.6	725.7	0.35
0.8	549.2	0.28
1.2	472.2	0.23
1.6	198.7	0.10

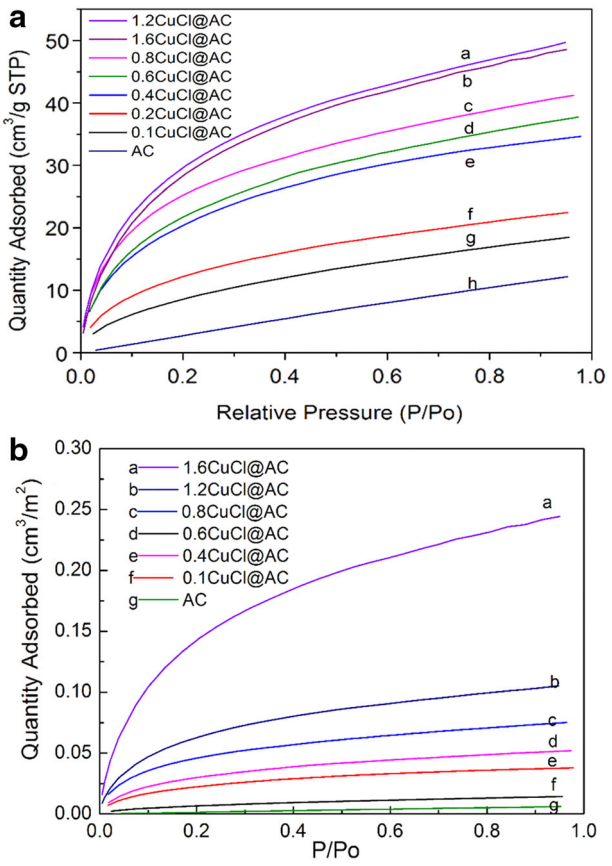

Fig. 1 **a** Isotherms of CO over CuCl@AC based on unit mass of adsorbents at 298 K, **b** Isotherms of CO over CuCl@AC based on unit BET surface area of adsorbents at 298 K

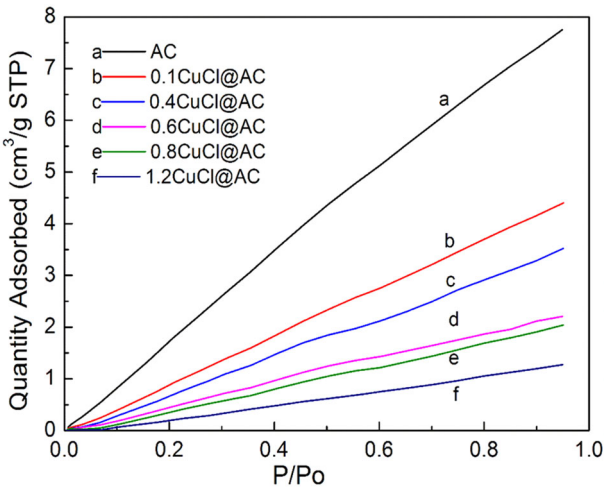

Fig. 2 Isotherms of N_2 over CuCl@AC adsorbents with different CuCl loadings at 298 K

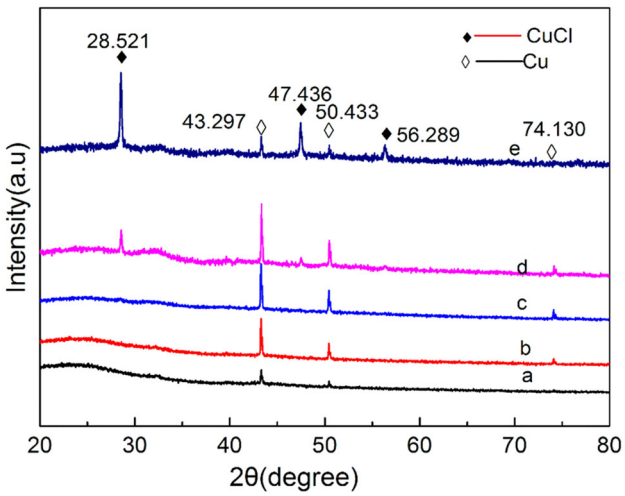

Fig. 3 XRD patterns of CuCl@AC adsorbents with different CuCl loadings (*a* 0.1, *b* 0.2, *c* 0.4, *d* 0.6, *e* 1.2)

In addition, we also calculated the utilization coefficient of surface CuCl, which is defined as: the CO equilibrium adsorption capacity/the ideal CO adsorption capacity (assuming one molar of CuCl on AC adsorbs one molar of CO). According to this definition, the utilization coefficients were calculated as 18.6 and 79.7 % for 1.2CuCl@AC and 0.1CuCl@AC, respectively at the P/P^0 of 0.9. It indicated that the high loading of CuCl on AC could not get the high utilization of CuCl. The reason was that not of all Cu species on the carbon surfaces were present in the form of Cu^+, which would be confirmed by XRD and XPS later.

Figure 2 shows isotherms of N_2 over CuCl@AC adsorbents with different CuCl loadings. In contrast to the case of CO adsorption on CuCl@AC adsorbents, The N_2 equilibrium adsorption capacities of the CuCl@AC adsorbents were lower than that of original AC, and decreased gradually with an increase in CuCl loading. It indicated that the loading of CuCl on AC greatly weaken N_2 adsorption on CuCl@AC adsorbents. With significantly enhanced CO adsorption capacity and decreased N_2 adsorption capacity after the loading of CuCl onto the original AC, CO/N_2 adsorption selectivity of CuCl@AC would be significantly enhanced, which will be discussed later.

Figure 3 shows the XRD patterns of CuCl@AC adsorbents with different CuCl loadings. It was visible that the characteristic XRD peaks of Cu^+ at 28.521, 47.436, and 56.289 occured, and the characteristic peaks of Cu^0 at 43.297, 50.433, and 74.130 occurred (Liu et al. 2002; Bian et al. 2010). It indicated the co-presence of Cu^+ and Cu^0 on CuCl@AC adsorbents. The co-present Cu^0 can be attributed to the reduction of part Cu^+ over carbon surface during sample calcination at 350 °C under argon since carbon itself served as the reducing agent (Beyer et al. 2009).

It was noted that no Cu^+ characteristic peak was observed at low CuCl loading (<0.4 g/g), which can be due to well dispersed Cu^+ on AC and the particle size of CuCl beyond the detection limit of XRD (Chen et al. 2010). By further increasing CuCl loading (0.4–1.2 g/g) on AC, the characteristic peaks for Cu^+ appeared and became shaper with a higher CuCl loading, suggesting the crystal size of CuCl became big enough to be detected by XRD with clear crystallinity.

3.3 Effect of calcination time on CO adsorption performance of CuCl/AC adsorbents

Figure 4 shows the adsorption isotherms of CO over the 0.4CuCl@AC adsorbents prepared with different calcination times. It was observed that the CO adsorption capacity of these adsorbents followed the order of $1 > 0.5 > 6 > 4 > 2$ h. It indicated that the 0.4CuCl@AC adsorbent prepared with calcination time of 1 h had the highest CO adsorption capacity among these adsorbents, which may be related to valence of copper on the surfaces of 0.4CuCl@AC. Figure 5 shows the XRD patterns of the 0.4CuCl@AC adsorbents. No characteristic peak of Cu^+ was observed, which could be ascribed to high dispersion of Cu(I) and thus the resulting small particle size of Cu(I) on AC was beyond the detection limit of XRD. However, characteristic peaks of Cu^0 at 43.297, 50.433, and 74.130 were observed indeed, and the intensity of these peaks became sharper with calcination time. It implied that the longer the calcination time, the bigger the Cu^0 particle size, reflected by the sharpness of the characteristic peaks of Cu^0.

XPS was carried out to obtain information on the elemental composition and valence state of Cu species. Figure 6 shows the complete XPS spectra of CuCl@AC adsorbents prepared with different calcination time. The

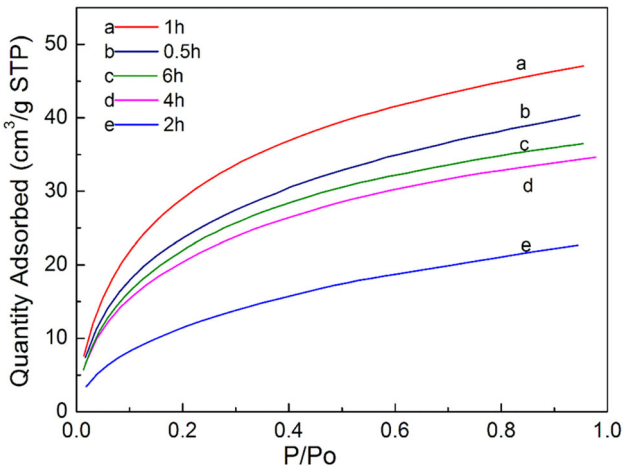

Fig. 4 Adsorption isotherms of CO over various 0.4CuCl@AC adsorbents prepared with different calcination time at 298 K

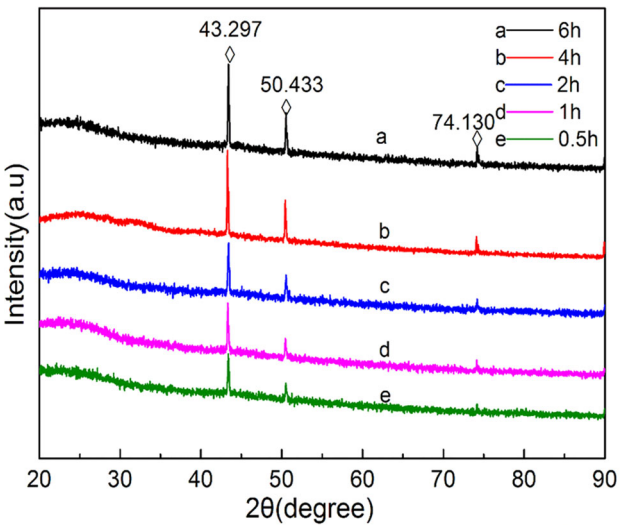

Fig. 5 XRD patterns of various 0.4CuCl@AC adsorbents prepared with different calcination time

peaks of Cu2p, O1s, C1s, and Cl2p were observed, suggesting the dominant elements on CuCl@AC adsorbents included Cu, O, C and Cl. That is to say, copper salt has been effectively loaded on the carbon surfaces. Figure 7 shows the XPS spectra of various CuCl@AC adsorbents at the binding energy range of various Cu states (925–965 eV). Characteristic peaks at 932.1 and 952.0 eV, respectively suggested the presence of Cu^+ and Cu^0 on CuCl@AC adsorbents. In addition, the characteristic peaks of Cu^{2+} at 953.6 and 933.4 eV, accompanied by the two satellite peaks were also observed. The presence of Cu^{2+} may be due to the oxidation of some CuCl during the initial mixing stage of preparating CuCl@AC adsorbents as CuCl is unstable and can be readily oxidized when exposed to air

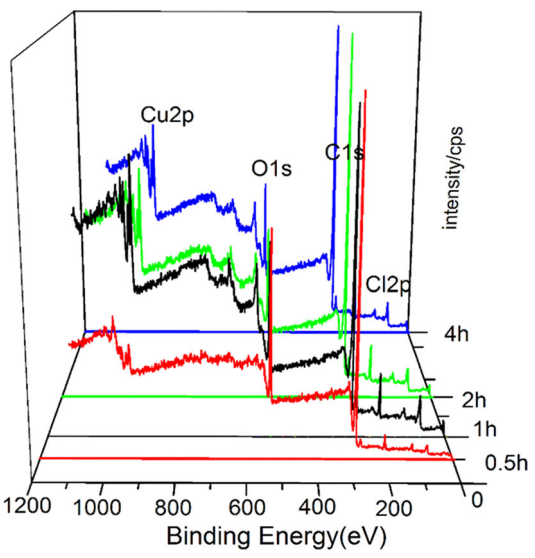

Fig. 6 The complete XPS spectra of 0.4CuCl@AC adsorbents prepared with different calcination time

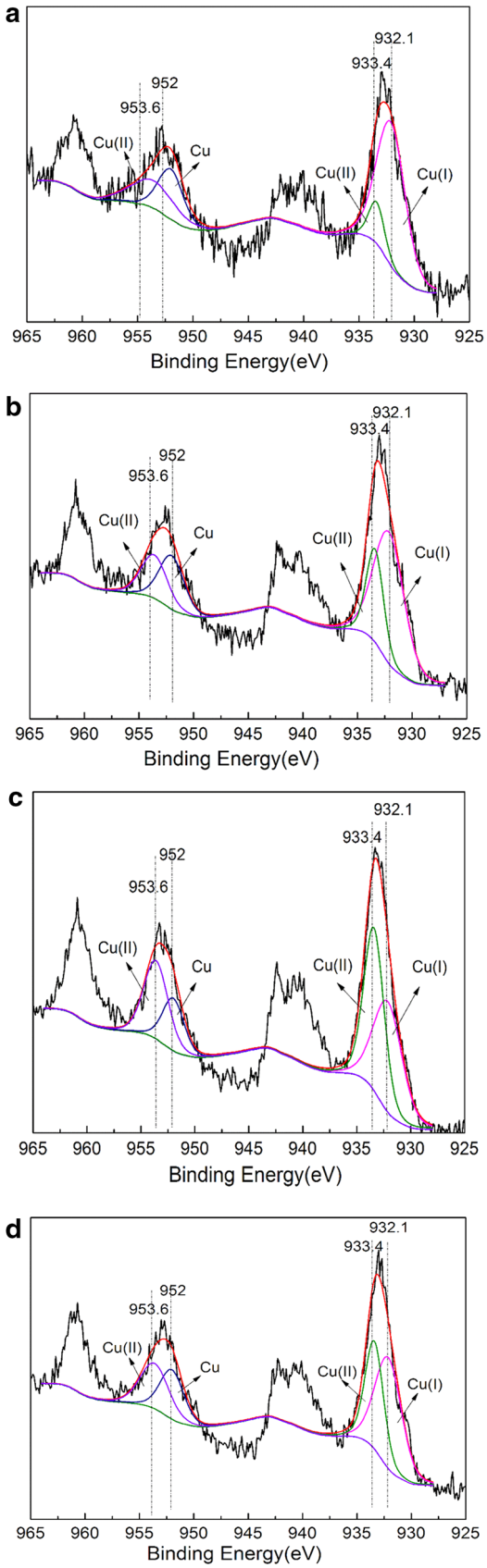

◀**Fig. 7** XPS spectra of various 0.4CuCl@AC adsorbents prepared with different calcination time (**a** 0.5 h, **b** 1 h, **c** 2 h, **d** 4 h)

or the partial oxidation of Cu^+ when handling the adsorbent for XPS characterization. The XPS patterns were derevoluted, and thus the percentages of Cu^+ on CuCl@AC adsorbents prepared with different calcination time were obtained, which were listed in Table 2. The data in Table 2 indicated that the percentages of Cu^+ on CuCl@AC adsorbents were 49.1, 56.4, 39.5, and 33.1 %, respectively for 0.5, 1, 2, and 4 h of calcination time, respectively. It follows the order of $1 > 0.5 > 6 > 4 > 2$ h, consistent with the order of CO adsorption capacity of CuCl@AC adsorbents prepared with different calcination time, as shown in Fig. 4. It suggested that the CuCl@AC adsorbents with high percentages of Cu^+ would have CO adsorption capacity since Cu^+ is a stronger adsorption site for CO than Cu species at other chemical states (Cu^0 and Cu^{2+}) on CuCl@AC adsorbents.

Noteworthy, the portion of Cu + increased from 49.1 to 56.4 % by increasing the calcination time from 0.5 to 1.0 h. The reason may be as follows. During preparation of Cu(I)@AC, there was co-present of Cu^{2+} on the surfaces of carbon due to the oxidation of some CuCl at the initial mixing stage as CuCl is unstable. Thus, during calcination, increasing the calcination time from 0.5 to 1.0 h at 350 °C under argon, a partial Cu^{2+} was reduced to Cu^+ and even Cu^0 as carbon itself served as the reducing agent (Beyer et al. 2009). As a result, when the calcination time increased from 0.5 to 1 h, percentage of Cu^{2+} (%) decreased from 35.4 to 26.3 %, and meanwhile, percentages of Cu^+ and Cu^0 increased separately from 49.1 to 56.4 % and from 15.5 to 17.3 %. However, increasing calcination time further would result in a decrease in percentages of Cu^+ on CuCl@AC adsorbents since some of Cu^+ was reduced to Cu^0 by carbon.

3.4 Adsorption selectivity of CO/N_2 over CuCl@AC

Besides adsorption capacity, adsorption selectivity plays an important role for the separation of gas mixtures. Herein, CO/N_2 adsorption selectivity was predicted by IAST (Myers and Prausnitz 1965; Rother and Fieback 2013; He et al. 2012). IAST assumes that the adsorbed mixture is an

Table 2 Percentages of Cu^+ on CuCl@AC adsorbents prepared with different calcination time

Calcination time	0.5 h	1 h	4 h	2 h
Percentage of Cu^+ (%)	49.1	56.4	39.5	33.1

ideal solution at constant spreading pressure and temperature, where the chemical potential of the adsorbed solution is considered to be equal to that of the gas phase at equilibrium (Zhang et al. 2011). To describe CO adsorption on the adsorbent with non-uniform and heterogeneous surface clearly, the dual-site Langmuir–Freundlich (DSLF) equation was used to fit a single-component isotherm (Huang et al. 2014), which can be expressed as

$$q = q_{m,1}\frac{b_1 p^{1/n_1}}{1 + b_1 p^{1/n_1}} + q_{m,2}\frac{b_2 p^{1/n_2}}{1 + b_2 p^{1/n_2}}$$

where p is the pressure of the bulk gas at equilibrium with the adsorbed phase (kPa); $q_{m,1}$ and $q_{m,2}$ are the saturation capacities of sites 1 and 2 (mmol/g), respectively; b_1 and b_2 are the affinity coefficients of sites 1 and 2 (1/kPa), respectively; and n_1 and n_2 are the corresponding deviations from an ideal homogeneous surface. Table 3 lists fitting parameters of the DSLF isotherm model for the pure isotherms of CO and N_2 on AC and 1.2CuCl@AC adsorbent. After these fitting parameters were obtained, the DSLF model was combined with IAST to predict the mixture adsorption isotherms and calculate the selectivities of the two samples for CO/N_2 adsorption.

Figure 8 presents the adsorption isotherms of CO and N_2 on AC and 1.2CuCl@AC as a function of the total bulk pressure. Compared to N_2, CO was preferentially adsorbed on both AC and 1.2 CuCl@AC samples. In a sharp contrast, the difference between CO and N_2 adsorption capacities of 1.2CuCl@AC was much greater than that of the original AC, which indicated a much higher CO/N_2 adsorption selectivity on 1.2CuCl@AC than on AC. This can be attributed to strong CO–Cu^+ pi-complexation on 1.2CuCl@AC.

Figure 9 presents the IAST-predicted selectivities of CO/N_2 of 1.2CuCl/AC adsorbent as a function of total bulk pressure. It shows that the selectivities of 1.2CuCl/AC adsorbent for CO/N_2 adsorption decreased with pressure. At low pressure range of 0–10 kPa, the CO/N_2 adsorption selectivity of 1.2CuCl/AC adsorbent was up to 100–450. At higher pressure range of 20–100 kPa, the CO/N_2 adsorption selectivity of 1.2 CuCl/AC adsorbent became low sharply with pressure, and however, remained in the range of 50–100. This can be attributed to the stronger interaction of the samples with CO compared to N_2. From the discussion above, it can be seen that 1.2CuCl/AC adsorbent had not only a high adsorption capacity for CO, but also a high CO/N_2 adsorption selectivity, which made it a promising adsorbent for the effective separation of CO/N_2 mixture.

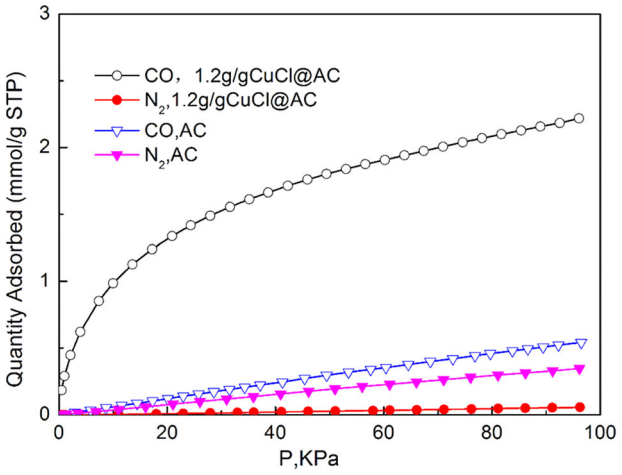

Fig. 8 Adsorption isotherms of CO and N_2 over original AC and 1.2CuCl@AC at 298 K

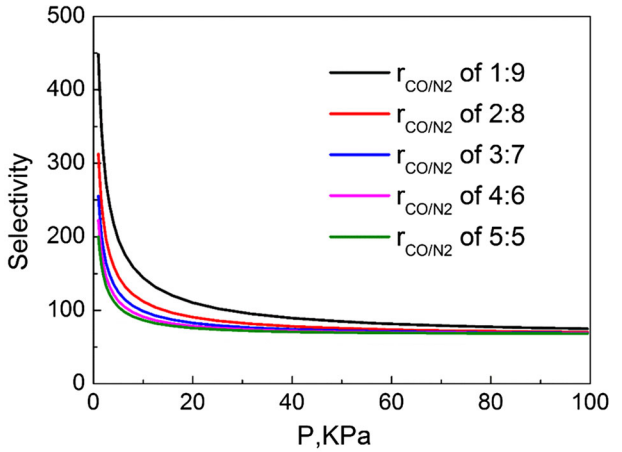

Fig. 9 IAST-predicted selectivities toward CO versus N_2 from CO/N_2 binary mixture at various CO/N_2 ratio ($r_{CO/N2}$) over the 1.2CuCl/AC adsorbent as a function of total bulk pressure at 273 K

4 Conclusions

A series of CuCl@AC adsorbents were successfully prepared for CO/N_2 separation using a solid-state auto dispersion method. With increasing CuCl loadings in the range of 0.0–1.2 g/g, the BET surface area of the prepared adsorbents CuCl@AC decreased, while their CO

Table 3 Equation parameters for the DSLF isotherm model

	$q_{m,1}$	b_1	n_1	$q_{m,2}$	b_2	n_2	R^2
CO	0.9315	0.1151	1.0492	57.8474	0.0033	2.2779	0.99995
N_2	2.6586	0.0005	1.2141	1.07180	0.0018	0.8560	0.99996

adsorption capacities increased. The maximal CO adsorption capacity of the CuCl@AC with CuCl loading of 1.2 g/g reached 38 cc/g at the P/P_0 of 0.40, around 8 times of that over the original AC. There was co-presence of Cu^{2+}, Cu^{+} and Cu^{0} on the surfaces of CuCl@AC. The co-present Cu^{2+} may came from the oxidation of some CuCl during the initial mixing stage of preparating CuCl@AC adsorbents as CuCl is unstable, and the co-present Cu^{0} can be attributed to the reduction of part Cu^{+} over carbon surface during sample calcination at 350 °C under argon since carbon itself served as the reducing agent. Calcination time for the preparation of Cu(I)@AC had significantly impact on CO adsorption of the adsorbents due to valence change of Cu species on carbon surfaces. XPS analysis indicated that when the calcination time was optimized to be 1 h at 350 °C under argon, the prepared Cu(I)@AC had the highest percentage of Cu^{+} species on its surfaces, and consequently it had the highest CO capacity among the adsorbents since adsorptive species responsible for CO adsorption is Cu^{+}. The dual-site Langmuir–Freundlich (DSLF) equation can fit isotherms of CO and N_2 vey well. The IAST-predicted CO/N_2 adsorption selectivities of 1.2CuCl/AC decreased with pressure. Its CO/N_2 selectivity was up to 100–450 at low pressure range of 0–10 kPa, and it remained in the range of 50–100 at higher pressure range of 20–100 kPa. The high adsorption capacity and selectivity of Cu(I)@AC adsorbents made it a promising adsorbent for CO/N_2 mixture separation.

Acknowledgments We gratefully acknowledge the financial support from China Tobacco Yunnan Industrial, Co., LTD through the research project of selective mitigation of hazardous components from Yunnan Tobacco by composite materials (2012FL03), and the State Key Laboratory of Subtropical Building Science, South China University of Technology (No. C714004z).

References

Al-Khatib, M.F., Iyuke, S.E., Mohamad, A.B.: The effect of impregnation of activated carbon with $SnCl_2H_2O$ on its porosity, surface composition and CO gas adsorption. Carbon **40**(11), 1929–1936 (2002)

Beyer, H., Chatziapostolou, K., Kohler, K.: Abatement of NO using rhodium catalysts supported on carbon nanotubes: carbon as support material and reducing agent. Top. Catal. **52**, 1752–1756 (2009)

Bian, J., Wei, X.W., Jin, Y.R., Wang, L., Luan, D.C., Guan, Z.P.: Direct synthesis of dimethyl cabonate over activated carbon supported Cu-based catalysts. Chem. Eng. J. **165**(2), 686–692 (2010)

Chavan, S., Vitillo, J.G., Groppo, E., Bonino, F., Lamberti, C., Dietzel, P.D., Bordiga, S.: CO adsorption on CPO-27-Ni coordination polymer: spectroscopic features and interaction energy. J. Phys. Chem. C **113**(8), 3292–3299 (2009)

Chen, Y.S., Xie, C., Li, Y., Song, C.S., Bolin, T.B.: Sulfur poisoning mechanism of steam reforming catalysts: an X-ray absorption near edge structure (XANES) spectroscopic study. Phys. Chem. Chem. Phys. **12**(21), 5707–5711 (2010)

Cheng, L.S., Yang, R.T.: Monolayer cuprous chloride dispersed on pillared clays for olefin-paraffin separations by pi-complexation. Adsorption **1**(1), 61–75 (1995)

Cho, S.H., Park, J.H., Han, S.S., Kim, J.N.: Comparison of $AgNO_3$/Clay and $AgNO_3$/ALSN sorbent for ethylene separation. Adsorption **11**(1), 145–149 (2005)

Chowdhury, P., Bikkina, C., Meister, D., Dreisbach, F., Gumma, S.: Comparison of adsorption isotherms on Cu-BTC metal organic frameworks synthesized from different routes. Microporous Mesoporous Mater. **117**(1–2), 406–413 (2009)

Chowdhury, P., Mekala, S., Dreisbach, F., Gumma, S.: Adsorption of CO, CO_2 and CH_4 on Cu-BTC and MIL-101 metal organic frameworks: effect of open metal sites and adsorbate polarity. Microporous Mesoporous Mater. **152**, 246–252 (2012)

Čičmanec, P., Bulánek, R., Frýdová, E., Kolářová, M.: Study of thermodynamic characteristics of CO adsorption on Li exchanged zeolites. Adsorption **19**(2–4), 381–389 (2013)

Czakkel, O., Onyestyak, G., Pilatos, G.: Kinetic and equilibrium separation of CO and CO_2 by impregnated spherical carbons. Microporous Mesoporous Mater. **120**(1–2), 76–83 (2009)

Delgado, M.R., Arean, C.O.: Carbon monoxide, dinitrogen and carbon dioxide adsorption on zeolite H-Beta: IR spectroscopic and thermodynamic studies. Energy **36**(8), 5286–5291 (2011)

García, E.J., Mowat, J.P., Wright, P.A., Pérez-Pellitero, J., Jallut, C., Pirngruber, G.D.: Role of structure and chemistry in controlling separations of CO_2/CH_4 and CO_2/CH_4/CO mixtures over honeycomb MOFs with coordinatively unsaturated metal sites. J. Phys. Chem. C **116**(50), 26636–26648 (2012)

Grande, C.A., Lopes, F.V., Ribeiro, A.M., Loureiro, J.M., Rodrigues, A.E.: Adsorption of Off-Gases from Steam Methane Reforming (H_2, CO_2, CH_4, CO and N_2) on Activated Carbon. Sep. Sci. Technol. **43**(6), 1338–1364 (2008)

He, P., Liu, H., Li, Y., Zhu, J., Huang, S., Lei, Z., Wang, P., Tian, H.: Adsorption of benzene and propene in zeolite MCM-22: a grand canonical Monte Carlo study. Adsorption **18**(1), 31–42 (2012)

Huang, W., Zhou, X., Xia, Q., Peng, J., Wang, H., Li, Z.: Preparation and adsorption performance of GrO@Cu-BTC for separation of CO_2/CH_4. Ind. Eng. Chem. Res. **53**, 11176–11184 (2014)

Iyuke, S.E., Daud, W.R.W., Mohamad, A.B., Kadhum, A.A.H., Fisal, Z., Shariff, A.M.: Application of Sn-activated carbon in pressure swing adsorption for purification of H_2. Chem. Eng. Sci. **55**(20), 4745–4755 (2000)

Izumi, J., Yasutake, A., Kobayashi, S., Shikichi, A., Kinugasa, A., Kohanawa, O., Okumura, M., et al.: ^{14}CO and ^{12}CO separation on Na-X using pressure swing adsorption at low temperatures. Adsorption **11**(1), 817–821 (2005)

Leclerc, H., Vimont, A., Lavalley, J.C., Daturi, M., Wiersum, A.D., Llwellyn, P.L., Horcajada, P., Férey, G., Serre, C.: Infrared study of the influence of reducible iron (III) metal sites on the adsorption of CO, CO_2, propane, propene and propyne in the mesoporous metal–organic framework MIL-100. Phys. Chem. Chem. Phys. **13**(24), 11748–11756 (2011)

Lithoxoos, G.P., Labropoulos, A., Peristeras, L.D., Kanellopoulos, N., Samios, J., Economou, J.G.: Adsorption of N_2, CH_4, CO and CO_2 gases in single walled carbon nanotubes: a combined experimental and Monte Carlo molecular simulation study. J Supercrit. Fluids **55**, 510–523 (2010)

Liu, Y., Hayakawa, T., Suzuki, K., Hamakawa, S., Tsunoda, T., Ishii, T., Kumagai, M.: Highly active copper/ceria catalysts for steam reforming of methanol. Appl. Catal. A **223**(1–2), 137–145 (2002)

Lopes, F.V., Grande, C.A., Ribeiro, A.M., Loureiro, J.M., Evaggelos, O., Nikolakis, V., Rodrigues, A.E.: Adsorption of H_2, CO_2, CH_4,

CO, N_2 and H_2O in activated carbon and zeolite for hydrogen production. Sep. Sci. Technol. **44**(5), 1045–1073 (2009)

Ma, J., Li, L., Ren, J., Li, R.: CO adsorption on activated carbon-supported Cu-based adsorbent prepared by a facile route. Sep. Purif. Technol. **76**(1), 89–93 (2010)

Miyajima, H., Kodama, A., Goto, M., Hirose, T.: Improved purge step in pressure swing adsorption for CO purification. Adsorption **11**(1), 625–630 (2005)

Munusamy, K., Sethia, G., Patil, D.V., Somayajulu Rallapalli, P.B., Somani, R.S., Bajaj, H.C.: Sorption of carbon dioxide, methane, nitrogen and carbon monoxide on MIL-101 (Cr): volumetric measurements and dynamic adsorption studies. Chem. Eng. J. **195**, 359–368 (2012)

Myers, A.L., Prausnitz, J.M.: Thermodynamics of mixed-gas adsorption. AIChE J. **11**, 121–127 (1965)

Park, Y., Moon, D.K., Kim, Y.H., Ahn, H., Lee, C.H.: Adsorption isotherms of CO_2, CO, N_2, CH_4, Ar and H_2 on activated carbon and zeolite LiX up to 1.0 MPa. Adsorption **20**(4), 631–647 (2014)

Rakić, V., Rac, V., Dondur, V., Auroux, A.: Competitive adsorption of N_2O and CO on CuZSM-5, FeZSM-5, CoZSM-5 and bimetallic forms of ZSM-5 zeolite. Catal. Today **110**(3), 272–280 (2005)

Rother, J., Fieback, T.: Multicomponent adsorption measurements on activated carbon, zeolite molecular sieve and metal-organic framework. Adsorption **19**(5), 1065–1074 (2013)

Sato, H., Kosaka, W., Matsuda, R., Hori, A., Hijikata, Y., Belosludov, R.V., Sakaki, S., Takata, M., Kitagawa, S.: Self-accelerating CO Sorption in a soft nanoporous crystal. Science **343**(6167), 167–170 (2014)

Sethia, G., Dangi, G.P., Jetwani, A.L., Somani, R.S., Bajaj, H.C., Jasra, R.V.: Equilibrium and dynamic adsorption of carbon monoxide and nitrogen on ZSM-5 with different SiO_2/Al_2O_3 ratio. Sep. Sci. Technol. **45**, 413–420 (2010)

Song, C.S.: Fuel processing for low-temperature and high-temperature fuel cells: challenges, and opportunities for sustainable development in the 21st century. Catal. Today **77**(1–2), 17–49 (2002)

Takahashi, A., Yang, F.H., Yang, R.T.: New sorbents for desulfurization by pi-complexation: thiophene/benzene adsorption. Ind. Eng. Chem. Res. **41**(10), 2487–2496 (2002)

Wirawan, S.K., Creaser, D.: Multicomponent $H_2/CO/CO_2$ adsorption on BaZSM-5 zeolite. Sep. Purif. Technol. **52**(2), 224–231 (2006)

Xiao, J., Li, Z., Liu, B., Xia, Q.B., Yu, M.X.: Adsorption of benzothiophene and dibenzothiophene on ion-impregnated activated carbons and ion-exchanged Y zeolites. Energy Fuels **22**(6), 3858–3863 (2008)

Xiao, J., Bian, G.A., Zhang, W., Li, Z.: Adsorption of dibenzothiophene on Ag/Cu/Fe-supported activated carbons prepared by ultrasonic-assisted impregnation. J. Chem. Eng. Data **55**(12), 5818–5823 (2010)

Xiao, J., Sitamraju, S., Chen, Y.S., Janik, M.J., Song, C.S.: Air-promoted adsorptive desulfurization (ADS) over $Ti_{0.9}Ce_{0.1}O_2$ mixed oxides from diesel fuel under ambient conditions. ChemCatChem **5**, 3582–3586 (2013)

Xiao, J., Sitamraju, S., Janik, M.J.: CO_2 adsorption thermodynamics over N-substituted/grafted graphanes: a DFT study. Langmuir **30**(7), 1837–1844 (2014)

Xie, Y.: Highly efficient CuCl/zeolite for CO adsorption. Chem. J. Chin. Univ. **18**, 1165–1169 (1997)

Yang, R.T., Hernandez-Maldonado, A.J., Yang, F.H.: Desulfurization of transportation fuels with zeolites under ambient conditions. Science **301**(5629), 79–81 (2003)

Yang, R.T., Wang, Y., Heinzel, J.M.: Desulfurization of jet fuel by pi-complexation adsorption with metal halides supported on MCM-41 and SBA-15 mesoporous materials. Chem. Eng. Sci. **63**(2), 356–365 (2008)

Zhang, Z., Xian, S.K., Xi, H.X., Wang, H.H., Li, Z.: Improvement of CO_2 adsorption on ZIF-8 crystals modified by enhancing basicity of surface. Chem. Eng. Sci. **66**, 4878–4885 (2011)